Volume 23, No 1 | International Journal of Radiation Research, January 2025

Usefulness of cast-type bolus produced by 3D printing for photon beam treatment of primary cutaneous lymphoma: A phantom experiment

Y. Won[1] and S. Kim[2*]

[1]*Department of Radiation Oncology, Uijeongbu Eulji Medical Center, Eulji University, Gyeonggi-do, South Korea*
[2]*Department of Radiological Science, Gachon University Medical Campus, Namdong-gu, Incheon, South Korea*

► ***Original article***

Corresponding author:
Sungchul Kim, Ph.D.,
E-mail: *ksc@gachon.ac.kr*

Received: October 2023
Final revised: March 2024
Accepted: June 2024

Int. J. Radiat. Res., January 2025; 23(1): 69-75

DOI: 10.61186/ijrr.23.1.69

Keywords: *Bolus, 3D printing, Photon beam, Intensity modulated radiotherapy.*

ABSTRACT

Background: To examine the usefulness of photon beam radiation therapy for primary cutaneous lymphoma, a phantom experiment was conducted by fabricating and applying an M3 casting type customized bolus by three-dimensional (3D) printing. ***Materials and Methods:*** Several 3D printers were used to compare output times according to division to reduce the output time of cast-type bolus. The dose distribution and dose verification for each treatment plan of electron beam (6 MeV, 9 MeV) and photon beams (AP/PA, field-in-field 3D conformal radiation therapy [3D CRT], intensity modulated radiotherapy [IMRT]) were analyzed. During photon beam treatment, the inside of the molded bolus was filled with rice and M3 for the experiment. ***Results:*** Compared with the infill type, the split casting type output method improved the output speed of the 3D printer by up to 94.7% and could be applied to patients within 48 h. Moreover, the treatment plan of the photon beam, compared with that of the 9 MeV electron beam, improved the radical dose homogeneity index (rDHI) by 23.0% to 71.3% and the moderate homogeneity index (mDHI) by 7.5% to 18.6% in the planning tumor volume, indicating a more uniform dose distribution. ***Conclusion:*** The difference in treatment plan evaluations between M3 and rice was similar, but in dose delivery, the maximum errors were 3.1% and 6.5%, respectively, indicating that M3 was superior to rice.

INTRODUCTION

Primary cutaneous lymphoma has a different prognosis than those of histologically similar systemic lymphoma, and various treatment methods are required because of the possibility of secondary occurrence in the skin [1]. The range of radiation therapy using electron beams for primary cutaneous lymphomas extends from the site of occurrence to the surrounding periphery, ranging from 0.5 to 5.0 cm. Typically, radiation therapy is applied within a range of £2.0 cm, and the treatment dose usually falls between 24 and 40 Gy [2-4].

Since electron beams have low penetrative power, they have an advantage in treating skin with few irregularities, but when the treatment area is wide or irregularities are present in the skin of the extremities, the homogeneity of the dose in the treatment area is reduced. Therefore, for lesions classified as T2b or higher, electron beams cannot be selected, leading to an increasing frequency of photon beam therapy [5-7].

During photon beam treatment, a bolus should be applied because the skin dose is insufficient. Furthermore, because of its high penetrative power, a phenomenon occurs in which the beam is delivered to deep tissues other than the skin. To prevent such issues, techniques such as intensity modulated radiotherapy (IMRT), volume modulated arc therapy (VMAT), and arc radiation therapy are employed to protect critical organs during radiation treatment [8].

During the treatment of primary cutaneous lymphomas, bolus materials such as gel tissue-equivalent (GTE), Vaseline gauze (VG), and rice have been traditionally used. However, the use of poly lactic acid (PLA) and acrylonitrile butadiene styrene (ABS) have increased with three-dimensional (3D) printing technology [6, 9-10]. The bolus conditions in primary cutaneous lymphoma treatment involve eliminating skin contour irregularities, ensuring adequate adherence to skin tissue, and maintaining uniform density within the bolus material while avoiding the presence of air gaps. Further, the time to make a bolus should be short, reproducibility should be maintained at each set-up, and the same shape should be maintained at least during the treatment period. However, conventional bolus materials pose issues in terms of air gap presence and reproducibility within the radiation therapy environment [11-15]. To solve these problems, a radiation treatment method has been developed with a photon beam after manufacturing a virtual bolus using a 3D printer. However, 3D printers are produced and applied in small sizes due to their long production times, which limits the application area of radiation therapy [9]. For radiation treatment of a

[DOI: 10.61186/ijrr.23.1.69]

wide range of primary cutaneous lymphomas, a large bolus must be rapidly produced. To increase the production speed of 3D printing, the inside of the structure may be emptied to reduce the amount of output and a substitute material may be constructed in the empty interior. Additional methods exist to increase the output speed and diameter of the nozzle and simultaneously output the divided structures [16,17].

We intended to apply boluses customized for the patients using M3, a material comprising paraffin wax (76.92%), magnesium oxide (22.35), calcium carbonate (0.72) [18], instead of rice boluses to address the limitations in manufacturing large boluses and time constraints encountered during radiation therapy for extensive primary cutaneous lymphoma. To expedite the fabrication of M3 boluses, the mold for M3 boluses was divided into four parts using a 3D printer. Additionally, to compare and evaluate the radiation therapy performance of the boluses, the interior of each mold was fabricated with rice or M3. We aimed to confirm the efficacy of each material for radiation therapy by applying radiation therapy and measuring the dose and dose distribution.

METHODS AND MATERIALS

Fabrication and material properties of phantoms and bolus

The leg phantom and bolus used for measurement were made with a 3D printer (3DP-310F, CUBICON, Korea), and the soft tissue of the leg phantom consisted of PLA (PLA Filament, CUBICON, Korea), M3 (paraffin wax: Eesy paraffin wax, Rang Pang, China; magnesium oxide: Samchun, Korea; calcium carbonate: Comscience, Korea), and growfill PLA (Glowfill, ColorFabb, Netherlands). The bolus was produced with a treatment planning system (TPS) (eclipse 8.6, Varian medial system, Palo Alto, CA, USA) in the form of a box with a sufficient thickness to accommodate build-up. The outer contour of the bolus was composed of PLA, and two boluses were made to allow the inner section to be composed of rice and M3, as shown in figure 1. One bolus was made with anterior and posterior sections to sufficiently cover and detach the phantom.

To examine the production time of the bolus and the reduction of production time when splitting output, the output time, split into two and four parts, was investigated. To confirm the physical properties of the phantom and bolus, the properties of the constituent materials, Rice, GTE, M3, PLA, and Growfill PLA, were measured three times with the Hounsfield unit (HU) using computed tomography (CT) (Light speed RT16, General Electric Healthcare, Milwaukee, WI, USA) imaging. Standard deviations (SDs) were then calculated.

Imaging

For the electron beam treatment plan, CT images were acquired after marking virtual lesions on the phantom with wires. Images were acquired in the same way for the photon beam treatment plan, but a bolus was additionally combined on the phantom. CT images were acquired, as shown in figure 2. The acquired images were transmitted to the TPS for treatment planning.

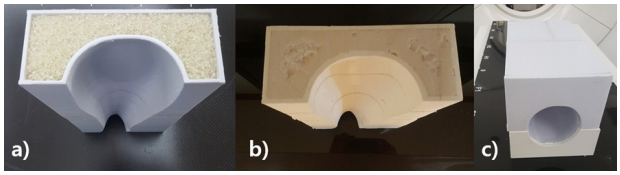

Figure 1. The inside of the bolus was filled with rice and M3. **a)** Rice, **b)** M3, **c)** anterior and posterior bolus from the left.

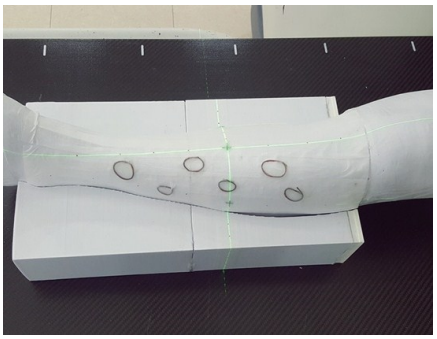

Figure 2. Gross tumor volume was marked with wires on the phantom.

Structure definition and treatment planning

In the transmitted CT image, the virtual lesion area was assumed to be the gross tumor volume (GTV) in the treatment planning system. Margin of 1.5 cm was sufficiently given for clinical tumor volume (CTV), and a 0.5 cm margin was given for planning tumor volume (PTV). The multi-leaf collimator (MLC) was set to a 0.5 cm margin.

Regarding electron beams, two treatment plans were created, including a one-port 6-MeV beam and a one-port 9 MeV beam using the 0.3 cm GTE bolus. The photon beam created three treatment plans using 6 MV. The created treatment plan involved a two-port AP/PA beam, four-port FIF 3D CRT beam (290˚, 330˚, 120˚, and 160˚ gantry angles), and five-port IMRT beam (290˚, 330˚, 45˚, 120˚, and 160˚ gantry angled).

The dose prescribed to the PTV was 40 Gy in 20 fractions. Photon treatment plans were compared after PTV normalization, so the average dose of PTV was 40 Gy. The treatment plan was determined using the analytical anisotropic algorithm (AAA).

Treatment plan evaluation

To evaluate the treatment plan for tumors, the homogeneity index (HI) of PTV for each treatment plan was calculated using the radical dose homogeneity index (rDHI) (equation 1) and moderate homogeneity index (mDHI) (equation 2), referring to the equations provided in [19].

$$rDHI = \frac{D_{\min}}{D_{\max}} \quad (1)$$

[DOI: 10.61186/ijrr.23.1.69]

Where; D_{min} is the minimum dose of PTV and D_{max} is the maximum

$$mDHI = \frac{D \geq 95\%}{D \geq 5\%} \quad (2)$$

Where; D ≥ 95% and D ≥ 5% are the doses delivered over 95% and 5% of the PTV volume in the radiation treatment plan, respectively.

Organs at risk were analyzed using the dose volume histogram (DVH) for each organ.

Dose verification

1) MOSFET dosimeter calibration: For dose verification, a metal-oxide-semiconductor field-effect transistor (MOSFET) (TN-502RD, T&N Electronics, Ontario, Canada) dosimeter was calibrated at the D_{max} point of the linear accelerator (LINAC) (Clinac ix, Varian Medical systems Inc., Palo Alto, CA, USA) by applying the IAEA-TRS 398 protocol [20]. The detailed conditions consisted of a photon beam of 6 MV, a field size of 10×10 cm^2, and sensors A and B of the MOSFET detector placed at the D_{max} point. A MOSFET linearity response curve was prepared by repeatedly irradiating sensors A and B with doses of 0.0, 0.1, 0.3, 0.5, 0.7, 1.0, 1.5, 2, 2.5, and 3 Gy, three times each [21-22]. The measured correlation coefficient was 0.9995, and the trend lines appeared as follows: A sensor Y = 1.0354X–1.2743 and B sensor Y = 1.0339X–1.5944. The phantom experiment measurement values were corrected by the trend line.

2) Dose measurement: The phantom and bolus were reproduced in the same way as the treatment plan in the radiation treatment room. The dose measurement point using MOSFET is shown in figure 3. The measurement sites of the phantom included three points. Point A was the anterior region, point B was the left region, and point C was the posterior region. AP/PA treatment plans were measured at points A and C, and FIF 3D CRT and IMRT treatment plans were measured at points A and B, repeated thrice.

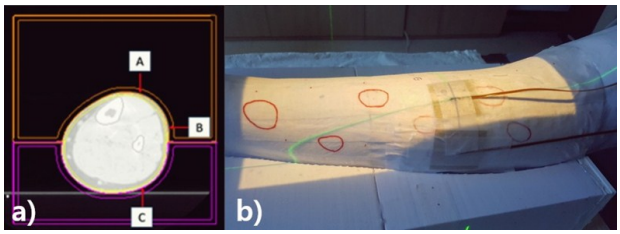

Figure 3. Dose measurement points of the phantom and MOSFET (metal-oxide-semiconductor field-effect transistor) sensor points. **a)** Measurement point of transverse image, **b)** measurement point of surface.

Data analysis

All dose data used for dose verification were calculated using the statistical package for the social sciences (version 22, IBM, Armonk, New York, USA) and the calculated doses were used to confirm the standard deviations of dose data measured in three repetitions.

RESULTS

Physical properties and 3D printer output time

1) Physical properties: The HU measurements of the bolus and phantom materials were as follows: rice, -116.6±116.7; GTE, -47.1±11.6; M3, 44.2±29.5; PLA, 161.2±18.3; and Growfill PLA, 330.2±24.3. GTE and M3 were found to be most similar to the human soft tissues, and Growfill was found to be similar to human bone. In addition, rice showed the greatest difference in standard error due to the difference in density between rice particles and air (table 1).

Table 1. Bolus material density and HU value

	Rice	GTE	M3	PLA	Growfill PLA
Density (g/cm^3)	0.84	1.03	1.05	1.24	1.20~1.43
HU	-116.6 ± 116.7	-47.1 ± 11.6	44.2 ± 29.5	161.2 ± 18.3	330.2 ± 24.3

GTE: gel tissue-equivalent; PLA: of poly lactic acid; HU: Hounsfield unit

2) 3D printer output time: The total bolus volume was 12,695 cm^3, which was measured as an anterior bolus volume of 7,909 cm^3 and a posterior bolus volume of 4,786 cm^3. The output times and amounts of the infill and casting types (5-mm thick PLA, internally empty) were 764.9 h and 16,905 g, and 275.8 h and 3,669 g, respectively, of the anterior and posterior bolus. The output time decreased by 63.9%, and the output amount decreased by 78.2%. Moreover, compared with the full casting type, the output time was reduced by 50% and 75% when printing in two or four divisions, respectively. When printing casts in four divisions, printing time could be reduced by up to 94.7%, compared with the infill casting (table 2).

Table 2. Output times of split, infill-type, and casting-type boluses

Type			Full	2-split	4-split
Infill type	Anterior	Time (h)	475.2	237.6	118.8
		Mass (g)	10,550	5,275	2,638
	Posterior	Time (h)	289.7	144.8	72.4
		Mass (g)	6,355	3,178	1,589
	Total	Time (h)	764.9	382.4	191.2
		Mass (g)	16,905	8,453	4,226
Molding type	Anterior	Time (h)	159.7	79.8	39.9
		Mass (g)	2,088	1,044	522
	Posterior	Time (h)	116.1	58.0	29.0
		Mass (g)	1,581	791	395
	Total	Time (h)	275.8	137.8	68.9
		Mass (g)	3,669	1,835	917

Treatment planning evaluation

The dose distributions of the 6 MeV and 9 MeV electron beams and AP/PA (Rice, M3), FIF 3D CRT (Rice, M3), and IMRT (Rice, M3) photon beams by treatment plan are shown in figure 4. The homogeneity of PTV was excellent in the following order: photon beams FIF 3D CRT, AP/PA, and IMRT, and electron beams 9 MeV and 6 MeV. Further, rDHI

[DOI: 10.61186/ijrr.23.1.69]

and mDHI are shown in Table 3. Based on the 9-MeV electron beam, the rDHI values of photon beams AP/PA (Rice, M3), FIF 3D CRT (Rice, M3), and IMRT (Rice, M3) improved by 58.8%, 23.0%, 70.0%, 71.3%, 45.3%, and 32.6%, respectively. Additionally, mDHI values were improved by 15.2%, 12.6%, 18.6%, 18.2%, 8.8%, and 7.5%, respectively.

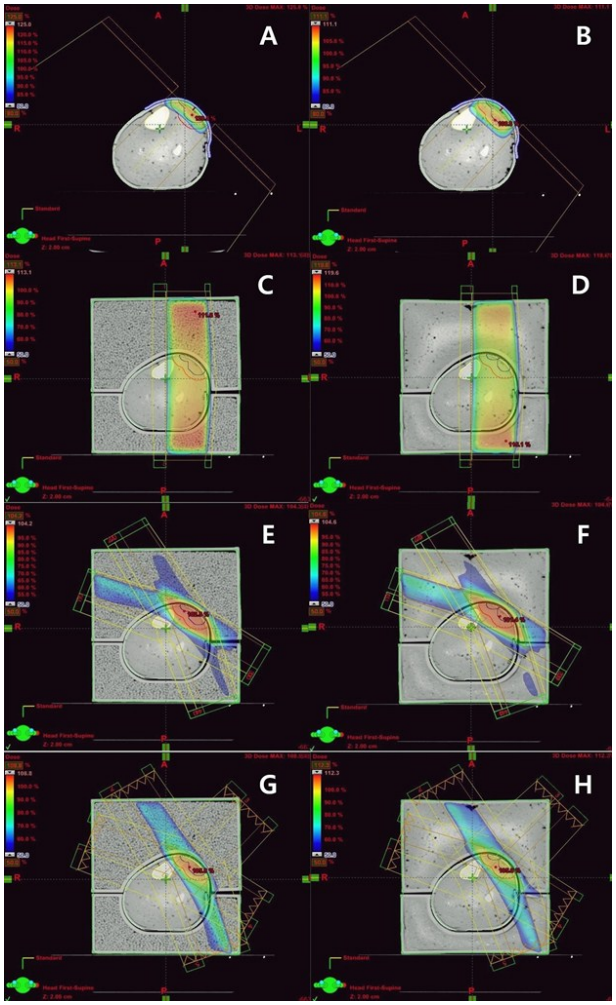

Figure 4. Dose distribution by treatment plan. **a)** Electron 6 MeV, **b)** electron 9 MeV, **c)** photon AP/PA rice bolus (AP/PA: anterior–posterior direction/posterior–anterior direction), **d)** Photon AP/PA M3 bolus, **e)** Photon FIF 3D CRT rice bolus (FIF 3D CRT: field-in-field 3D conformal radiation therapy), **f)** Photon FIF 3D CRT M3 bolus, **g)** Photon IMRT rice bolus (IMRT: intensity modulated radiation therapy), **h)** Photon IMRT M3 bolus.

Table 3. Planning tumor volume homogeneity index of the bolus material according to the treatment plan

Treatment planning		Material	rDHI	mDHI
Electron	6 MeV	GTE	0.068	0.311
	9 MeV	GTE	0.520	0.809
Photon (6 MV)	AP/PA	Rice	0.826	0.932
		M3	0.640	0.911
	FIF 3D CRT	Rice	0.884	0.960
		M3	0.891	0.957
	IMRT	Rice	0.756	0.881
		M3	0.690	0.870

rDHI: radical dose homogeneity index; mDHI: moderate homogeneity index; AP/PA: anterior–posterior direction/posterior–anterior direction; FIF 3D CRT: field-in-field 3D conformal radiation therapy; IMRT: intensity modulated radiation therapy

The DVH of each organ analyzed through radiation therapy plans and bolus data is presented in figure 5. The DVH, excluding the PTV treated with the 6 MeV electron beam, was normalized to 40% of the prescription dose of the PTV for comparison. As observed in table 3, the PTV in figure 5 exhibits superior homogeneity index in the order of FIF 3D CRT, AP/PA, and IMRT, with similar differences in treatment plans between the rice and M3 boluses.

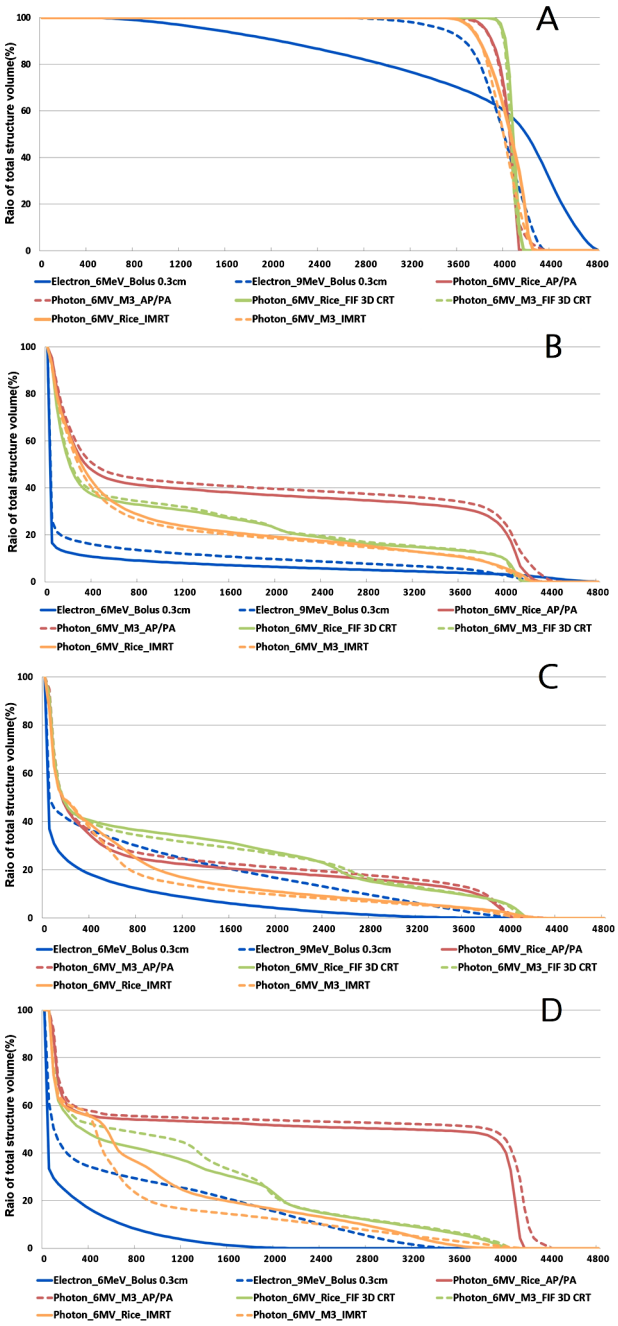

Figure 5. DVH by treatment plan (DVH: dose volume histogram). **a)** PTV DVH by treatment plan (PTV: planning tumor volume); **b)** leg body DVH by treatment plan; **c)** tibia DVH by treatment plan; **d)** fibula DVH by treatment plan.

The DVH values of the organs at risk (OAR) in the phantom leg were superior in the following order: 6-MeV electron beam, 9-MeV electron beam, IMRT photon beam, FIF 3D CRT photon beam, and AP/PA

[DOI: 10.61186/ijrr.23.1.69]

photon beam. In the tibia, the 6-MeV electron beam and IMRT photon beam were superior to the 9-MeV electron beam. The dose variation in treatment plans according to the material of the OAR showed a tendency for rice to be superior in the AP/PA and FIF 3D CRT treatment plans, while the M3 bolus showed superiority in the IMRT treatment plan.

Dose verification

Based on the A and C measurement points of rice during AP/PA treatment planning, the phantom doses were 198.9±2.4 cGy and 209.9±1.6 cGy, with error rates of -1.9% and -2.0%, respectively. The measurements of M3 were 204.7±1.6 cGy and 225.3±4.7 cGy, with error rates of 1.6% and 2.5%, respectively. Based on the A and B measurement points of rice during FIF 3D CRT treatment planning, the phantom doses were 197.3±1.2 cGy and 187.7±2.8 cGy, with error rates of -0.3% and –4.8%, respectively. M3 displayed similar trends with measurements of 196.3±4.8 cGy and 189.0±2.8 cGy, and error rates of 0.3% and -4.3%, respectively. Based on the A and B measurement points of rice during IMRT treatment planning, the phantom doses were 177.0±0.5 cGy and 159.3±2.7 cGy, with error rates of -2.9% and -6.5%, respectively. Those of M3 were 192.5±2.0 cGy and 178.8±2.0 cGy, with error rates of 3.1% and -0.1%, respectively.

By substance, the error measurements of rice increased as the treatment plan became more complicated than that of M3 (table 5).

Table 4. Dosimetry results by measurement location according to the treatment plan of rice and M3 bolus.

Material	Plan	Measure point	Plan dose (cGy)	Measurement dose (cGy)	Error percentage (%)
Rice	AP/PA	A	202.8	198.9±2.4	-1.9
		C	214.2	209.9±1.6	-2.0
	FIF 3D CRT	A	197.8	197.3±1.2	-0.3
		B	197.2	187.7±2.8	-4.8
	IMRT	A	182.2	177.0±0.5	-2.9
		B	170.4	159.3±2.7	-6.5
M3	AP/PA	A	201.4	204.7±1.6	1.6
		C	219.8	225.3±4.7	2.5
	FIF 3D CRT	A	195.8	196.3±4.8	0.3
		B	197.4	189.0±2.8	-4.3
	IMRT	A	186.8	192.5±2.0	3.1
		B	178.8	178.7±2.0	-0.1

DISCUSSION

Primary cutaneous lymphoma is treated with 6 or 9 MeV electron beams according to guidelines, but due to problems such as the range of treatment or unevenness, photon beams are sometimes treated using rice and other materials [1-3, 23]. Rice is useful for simple segment 3D CRT due to particles and empty space, but it can increase uncertainty in complex segment IMRT or VMAT, so a homogeneous bolus like M3 can be useful. The disadvantage of applying a customized bolus to photon beam therapy with a 3D printer is that it takes a very long time to manufacture, making patient application difficult.

When filling the inside of a large-capacity output object, like that in this experiment, to 100% and outputting with one 3D printer, the anterior and posterior bolus output times require 764.9 h. Since radiation therapy is generally applied within 2 to 3 days after CT simulation, it cannot be applied to patients in an internal 100% method. Therefore, methods to reduce the printing time must be devised, and printing time can be reduced by 63.9% by emptying the inside. However, even with this method, the output time is 275.8 h, which makes the structure impossible to apply to patients. Therefore, to apply this technology to patients, the split output method must be used. Ehler dramatically reduced output times using split outputs and increased nozzle sizes [16]. In this case, multiple 3D printers were required for simultaneously outputs. In this experiment, eight 3D printers could be used simultaneously and applied within 48 h; with four 3D printers, it could be applied within 72 h.

With complex treatment planning, FIF 3D CRT and IMRT were excellent in terms of DVH of PTV. Compared with the 9 MeV electron beam, the rDHI of PTV improved from 23% to 71.3%, and mDHI improved from 7.5% to 18.6% for each treatment plan using photon beams. The difference in doses between rice and M3 treatment plans according to materials was similar, although M3 was superior to rice, with HU values ranging from -116.6±116.7 to 48.1±29.4.

According to the study by Varadhan *et al.* [24], the uncertainty of all measurement processes of the MOSFET dosimeter was within ± 4.6% in total. The dose verification used in this experiment showed a similar tendency depending on the materials of AP/PA and FIF 3D CRT, and they were accurately measured within ± 3.0%, up to -4.8%. However, the error percentages of IMRT A and B measurement points were -2.9% and -6.5% for rice and 3.1% and -0.1% for M3, indicating that the error percentage of rice was increased. The MOSFET dosimeter had a direction dependency of < 2% when delivering doses under the same build-up conditions as those in this experiment, and the error was small even when a complicated treatment plan was used [21-22, 24-26].

The sharp drop in the measured values of the rice treatment plan in IMRT are thought to be due to the difference in standard deviations of the materials in the beam sequences of IMRT and the arrangement changes of rice in the process of moving from the CT simulation room to the radiation treatment room. In the same complex treatment plan, M3 more stably delivered the beam, compared with rice.

However, the M3 bolus can only be manufactured

[DOI: 10.61186/ijrr.23.1.69]

with a mold, and since the mold must be created with a 3D printer, even if multiple 3D printers are used, a time limit exists in applying it directly to the patient. Furthermore, since PLA and M3 are hard materials without elasticity, they may not be flexibly coped with patients' bodies. Recently, thermoplastic polyurethane has been used as a material to solve this problem [27, 28]. In particular, to treat total skin electron irradiation (TSEI) with photons, one method to improve skin dose uses a full-body wetsuit that is easy to apply to patients [29].

Furthermore, transparent boluses with enhanced visibility are being developed [30, 31]. Owing to transparency, these boluses, unlike conventional ones, allow for the monitoring of skin conditions and ink markers even when attached to the skin. This improves treatment planning and positional accuracy before confirming the patient's position by imaging, thereby enabling more precise radiation therapy for dermatological conditions without the need for Image-Guided Radiation Therapy. In particular, Adamson's polymeric gel bolus, possessing thermoplastic characteristics, enables shaping into desired forms upon heating, implying the feasibility of personalized bolus fabrication for individual patients [31]. Therefore, it is anticipated that future research combining the advantages of cutting-edge technologies will lead to the development of a limitless variety of boluses in terms of shape and material.

CONCLUSION

In the photon beam radiation treatment plan, compared with the infill type, the split casting method improved the output speed of the 3D printer by up to 94.7% and could be applied to patients within 48 h. Moreover, M3 has no internal material movement and is uniform, compared with rice, so in complex treatment plans such as IMRT, materials like M3 offer superior dose delivery.

ACKNOWLEDGMENT

We would like to thank Editage (www.editage.co.kr) for the English language editing.

Ethical Considerations: For this article no studies with human participants or animals were performed by any of the authors.

Funding: None.

Conflicts of Interest: The authors declare no conflicts of interest.

Author contributions: Conceptualization and methodology, Y.W. and S.K.; data collection, analysis, and interpretation of results, Y.W.; writing-original draft preparation, Y.W. and S.K.; writing review and editing, Y.W. and S.K. All authors have read and agreed to the published version of the manuscript.

REFERENCES

1. Jaffe ES, Harris NL, Stein H, Vardiman JW. Pathology and genetics of tumours of haematopoietic and lymphoid tissues. Lyon, France: IARC Press; 2001.
2. Specht L, Dabaja B, Illidge T, Wilson LD, Hoppe RT (2015) International Lymphoma Radiation Oncology Group. Modern radiation therapy for primary cutaneous lymphomas: field and dose guidelines from the International Lymphoma Radiation Oncology Group. *Int J Radiat Oncol Biol Phys,* ***92****(1): 32-9.*
3. Senff NJ, Noordijk EM, Kim YH, Bagot M, Berti E, Cerroni L, *et al.* (2008) European Organization for Research and Treatment of Cancer; International Society for Cutaneous Lymphoma. European Organization for Research and Treatment of Cancer and International Society for Cutaneous Lymphoma consensus recommendations for the management of cutaneous B-cell lymphomas. *Blood,* ***112****(5): 1600-09*.
4. Smith BD, Glusac EJ, McNiff JM, Smith GL, Heald PW, Cooper DL, *et al*. (2004) Primary cutaneous B-cell lymphoma treated with radiotherapy: a comparison of the European Organization for Research and Treatment of Cancer and the WHO classification systems. *J Clin Oncol,* ***22****(4): 634-9*.
5. Maingon P, Truc G, Dalac S, Barillot I, Lambert D, Petrella T, *et al*. (2000) Radiotherapy of advanced mycosis fungoides: indications and results of total skin electron beam and photon beam irradiation. *Radiother Oncol,* ***54****(1): 73-8.*
6. Majithia L, Rong Y, Siddiqui F, Hattie T, Gupta N, Weldon M, *et al*. (2015) Treating cutaneous T-cell lymphoma with highly irregular surfaces with photon irradiation using rice as tissue compensator. *Front Oncol,* ***5****: 49.*
7. Ahn KS, Jung WC, Kim DH, Kim MS, Yoon DK, Shim JG, *et al*. (2019) Evaluation of the Usefulness of Patient Customized Shielding Block Made with 3D Printer in the Skin Cancer Electron Beam Therapy. *J Radiol Sci Technol,* ***42****(6): 447-54.*
8. Song JH, Jung JY, Park HW, Lee GW, Chae SM, Kay CS, *et al.* (2015) Dosimetric comparison of three different treatment modalities for total scalp irradiation: the conventional lateral photon-electron technique, helical tomotherapy, and volumetric-modulated arc therapy. *J Radiat Res,* ***56****(4): 717-26*.
9. Kim SW, Kwak JW, Cho BC, Song SY, Lee SW, Jeong CY (2017) Clinical implementation of 3D Printing in the construction of patient specific bolus for photon beam radiotherapy for mycosis fungoides. *Prog Med Phys,* ***28****(1): 33-8.*
10. Vyas V, Palmer L, Mudge R, Jiang R, Fleck A, Schaly B, *et al*. (2013) On bolus for megavoltage photon and electron radiation therapy. *Med Dosim,* ***38****(3): 268-73*.
11. Michiels S, Barragán AM, Souris K, Poels K, Crijns W, Lee JA, *et al*. (2018) Patient-specific bolus for range shifter air gap reduction in intensity-modulated proton therapy of head-and-neck cancer studied with Monte Carlo based plan optimization. *Radiother Oncol,* ***128****(1): 161-6*.
12. Pugh R, Lloyd K, Collins M, Duxbury A (2017) The use of 3D printing within radiation therapy to improve bolus conformity: A literature review. *J Radiother Pract,* ***16****(3): 319-25.*
13. Humphries SM, Boyd K, Cornish P, Newman FD (1996) Comparison of super stuff and paraffin wax bolus in radiation therapy of irregular surfaces. *Med Dosim,* ***21****(3): 155-7.*
14. Sharma SC and Johnson MW (1993) Surface dose perturbation due to air gap between patient and bolus for electron beams. *Med Phys,* ***20****: 377-8*.
15. Khan YJ, Barajas E, Udowicz M, Sinha R, Muhammad W, Abbasi AN, *et al*. (2013) Clinical and dosimetric implications of air gaps between bolus and skin surface during radiation therapy. *J Cancer Ther,* ***4****(7): 1251-55.*
16. Ehler E, Sterling D, Dusenbery K, Lawrence J (2018) Workload implications for clinic workflow with implementation of three-dimensional printed customized bolus for radiation therapy: a pilot study. *PLoS One, 13(10): e0204944.*
17. Holtzer NA, Galis J, Paalman MI, Heukelom S (2014) 3D printing of tissue equivalent boluses and molds for external beam radiotherapy. *Radiother Oncol,* ***111****(1): S279*.
18. White DR (1978) Tissue substitutes in experimental radiation physics. *Med phys,* ***5****(6): 467–79.*
19. Oliver M, Chen J, Wong E, Dyk JV, Perera F (2007) A treatment planning study comparing whole breast radiation therapy against conformal, IMRT and tomotherapy for accelerated partial breast irradiation. *Radiother Oncol,* ***82****(3): 317-23*.
20. Technical Report Series No. 398. Absorbed dose determination in

[DOI: 10.61186/ijrr.23.1.69]

external beam radiotherapy: an international code of practice for dosimetry based on Standards of Absorbed Dose to Water. Vienna. 2000.
21. Ramaseshan R, Kohli KS, Zhang TJ, Lam T, Norlinger B, Hallil A, *et al*. (2004) Performance characteristics of a microMOSFET as an in vivo dosimeter in radiation therapy. *Phys Med Biol,* ***49****(17): 4031-48.*
22. Kumar AS, Sharm, SD, Ravindran BP (2014) Characteristics of mobile MOSFET dosimetry system for megavoltage photon beams. *J Med Phys,* ***39****(3): 142-9*.
23. Kim YH, Willemze R, Pimpinelli N, Whittaker S, Olsen EA, Ranki A, *et al*. (2007) TNM classification system for primary cutaneous lymphomas other than mycosis fungoides and Sezary syndrome: a proposal of the International Society for Cutaneous Lymphomas (ISCL) and the Cutaneous Lymphoma Task Force of the European Organization of Research and Treatment of Cancer (EORTC). *Blood,* ***110****(2): 479-84.*
24. Varadhan R, Miller J, Garrity B, Weber M (2006) *In vivo* prostate IMRT dosimetry with MOSFET detectors using brass buildup caps. *J Appl Clin Med Phys,* ***7****(4): 22-32*.
25. Consorti R, Petrucci A, Fortunato F, Soriani A, Marzi S, Iaccarino G, *et al.* (2005) In vivo dosimetry with MOSFETs: dosimetric characterization and first clinical results in intraoperative radiotherapy. *Int J Radiat Oncol Biol Phys,* ***63****(3): 952-60.*
26. Rudat V, Nour A, Alaradi AA, Mohamed A, Altuwaijri S (2014) *In vivo* surface dose measurement using GafChromic film dosimetry in breast cancer radiotherapy: comparison of 7-field IMRT, tangential IMRT and tangential 3D-CRT. *Radiat Oncol,* ***9****(1): 156*.
27. Wang H, Pi Y, Liu C, Wing X, Guo Y, Lu L, *et al*. (2023) Investigation of total skin helical tomotherapy using a 3D-printed total skin bolus. *Biomed Eng Online,* ***22****(1): 57*.
28. Song R and Li W (2023) 3D printed customized bolus for intensity-modulated radiotherapy in a patient with nasal radiotherapy. *International Journal of Radiation Research,* ***21****(1): 153-157.*
29. Wang H, Pi Y, Guo Y, Pei X, Xu X (2022) Influencing factors of total skin irradiation with helical tomotherapy. *Front Oncol,* ***12****: 852345*.
30. Son J, Jung S, Park J, Choi C, Kim J (2021) Assessing commercial CLEANBOLUS based on silicone for clinical use. *Progress in Medical Physics,* ***32****(4): 159-164.*
31. Adamson J, Cooney T, Demehri F, Stalnecker A, Georgas D, Yin F, *et al.* (2017) Characterization of water-clear polymeric gels for use as radiotherapy bolus. *Technology in cancer research & treatment,* ***16****(6): 923-929.*

[DOI: 10.61186/ijrr.23.1.69]